

# Chirality in the Kagome Metal $\text{CsV}_3\text{Sb}_5$

H.J. Elmers,<sup>1,\*</sup> O. Tkach,<sup>1,2</sup> Y. Lytvynenko,<sup>1,3</sup> P. Yogi,<sup>1</sup> M. Schmitt,<sup>4,5</sup> D. Biswas,<sup>4</sup> J. Liu,<sup>4</sup>  
S. V. Chernov,<sup>6</sup> M. Hoesch,<sup>6</sup> D. Kutnyakhov,<sup>6</sup> N. Wind,<sup>6,7</sup> L. Wenthaus,<sup>6</sup> M. Scholz,<sup>6</sup>  
K. Rossnagel,<sup>7,8</sup> A. Gloskovskii,<sup>6</sup> C. Schlueter,<sup>6</sup> A. Winkelmann,<sup>9</sup> A.-A. Haghighirad,<sup>10</sup> T.-L. Lee,<sup>4</sup>  
M. Sing,<sup>5</sup> R. Claessen,<sup>5</sup> M. Le Tacon,<sup>10</sup> J. Demsar,<sup>1</sup> G. Schönhense,<sup>1</sup> and O. Fedchenko<sup>1</sup>

<sup>1</sup>*Institut für Physik, Johannes Gutenberg-Universität, Staudingerweg 7, D-55128 Mainz, Germany*

<sup>2</sup>*Sumy State University, Kharkivska 116, 40007 Sumy, Ukraine*

<sup>3</sup>*Institute of Magnetism of the NAS and MES of Ukraine, 03142 Kyiv, Ukraine*

<sup>4</sup>*Diamond Light Source Ltd., Didcot OX11 0DE, United Kingdom*

<sup>5</sup>*Physikalisches Institut and Würzburg-Dresden Cluster of Excellence ct.qmat,  
Julius-Maximilians-Universität, D-97074 Würzburg, Germany*

<sup>6</sup>*Deutsches Elektronen-Synchrotron DESY, 22607 Hamburg, Germany*

<sup>7</sup>*Institut für Experimentelle und Angewandte Physik,*

*Christian-Albrechts-Universität zu Kiel, 24098 Kiel, Germany*

<sup>8</sup>*Ruprecht Haensel Laboratory, Deutsches Elektronen-Synchrotron DESY, 22607 Hamburg, Germany*

<sup>9</sup>*Academic Centre for Materials and Nanotechnology,*

*AGH University of Krakow, 30059 Kraków, Poland*

<sup>10</sup>*Institute for Quantum Materials and Technologies,*

*Karlsruhe Institute of Technology, 76021 Karlsruhe, Germany*

(Dated: August 8, 2024)

Using x-ray photoelectron diffraction (XPD) and angle-resolved photoemission spectroscopy, we study photoemission intensity changes related to changes in the geometric and electronic structure in the kagome metal  $\text{CsV}_3\text{Sb}_5$  upon transition to an unconventional charge density wave (CDW) state. The XPD patterns reveal the presence of a chiral atomic structure in the CDW phase. Furthermore, using circularly polarized x-rays, we have found a pronounced non-trivial circular dichroism in the angular distribution of the valence band photoemission in the CDW phase, indicating a chirality of the electronic structure. This observation is consistent with the proposed orbital loop current order. In view of a negligible spontaneous Kerr signal in recent magneto-optical studies, the results suggest an antiferromagnetic coupling of the orbital magnetic moments along the  $c$ -axis. While the inherent structural chirality may also induce circular dichroism, the observed asymmetry values seem to be too large in the case of the weak structural distortions caused by the CDW.

Kagome systems have recently attracted interest because of their unique electronic band structure, which exhibits delocalized electrons, Dirac points, flat bands, and multiple van Hove singularities (vHS) near the Fermi level [1–4]. The large density of states near vHSs can promote various electronic orders, such as superconductivity, chiral charge density wave (CDW), and orbital loop current order [5–8]. The vHSs in combination with flat bands can be the origin of correlated many-body ground states [9–14]. In particular, the kagome metals  $\text{AV}_3\text{Sb}_5$  ( $A = \text{K}, \text{Rb}, \text{Cs}$ ) combine unconventional charge orders [15–21], superconductivity [22–29], lattice frustration, and non-trivial topology [30–32]. Spectroscopic evidence for topological properties and correlation effects have been provided by ARPES studies [29, 33] and density functional theory [34–38]. In particular, the charge order has been related to time-reversal symmetry breaking (TRS) [16, 22, 30, 31] or rotational symmetry breaking [17, 18, 21].

In the normal high temperature state,  $\text{AV}_3\text{Sb}_5$  is a topological metal [29, 39] with topologically protected surface states near the Fermi level [29]. In the low temperature CDW state, scanning tunneling spectroscopy (STM) [31] and theory [36] have suggested a chiral CDW

order that breaks the time-reversal symmetry [36]. Observations of an anomalous Hall effect [32, 40–42] together with muon spin relaxation [30, 43] and magneto-optical Kerr effect (MOKE) studies [16, 44, 45] provided further evidence for the spontaneous time-reversal symmetry breaking. However, recent dedicated MOKE studies with zero-loop Sagnac interferometers [46–48] and STM [49] conclude that the occurrence of time-reversal symmetry breaking is unlikely.

Here, we use electron momentum microscopy to gain further insight into the structural and electronic chiral order in this system. Hard x-ray photoelectron diffraction (XPD) reveals a chiral order in the atomic structure in the CDW phase. On the other hand, photoelectrons excited by circularly polarized light in the soft x-ray region show spontaneous chiral symmetry breaking in the valence band states, which is particularly pronounced at certain mirror symmetry points in reciprocal space (*i.e.* M-points). We discuss time-reversal symmetry breaking or mirror symmetry breaking as possible origins for the observed effects.

The experiments were performed on single crystals of  $\text{CsV}_3\text{Sb}_5$  grown by the flux method and characterized by x-ray diffraction and energy-dispersive x-ray analy-

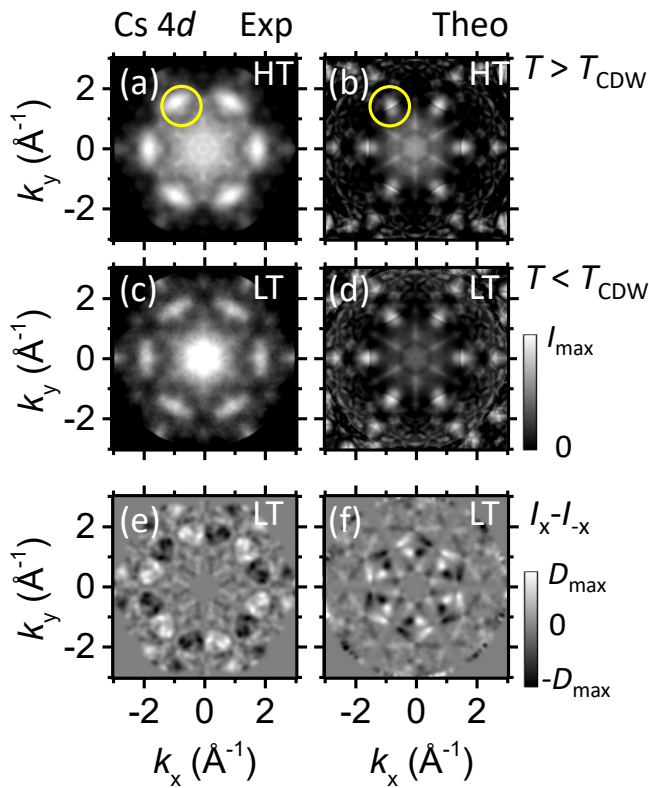


FIG. 1. X-ray photoelectron diffraction of  $\text{CsV}_3\text{Sb}_5$  measured at a photon energy of 6 keV for  $T > T_{\text{CDW}}$  (HT, 115 K) and  $T < T_{\text{CDW}}$  (LT, 30 K). Comparison of experimental (a,c) and theoretical (b,d) data. (e) Difference between the original data from (c) and the same data but mirrored at  $k_x = 0$  to highlight the broken mirror symmetry. (f) Similar data for the calculated results (see SM [51] for HT and other core levels).

sis [15, 50]. The  $\text{CsV}_3\text{Sb}_5$  structure and the experimental geometries for the photoemission experiments are given in the Supplemental Material (SM) [51]. The single crystals were freshly cleaved in ultrahigh vacuum.

$\text{CsV}_3\text{Sb}_5$  shows a CDW reconstruction below the transition temperature ( $T_{\text{CDW}} = 94$  K) [2]. To study the CDW-induced changes in the crystal structure we used core level XPD. Experiments in the hard x-ray range at 6 keV were performed at the time-of-flight momentum microscopy endstation of the hard x-ray beamline P22 at PETRA III [52]. The angle of incidence was  $\theta = 10^\circ$  with respect to the sample plane and the energy resolution was set to 600 meV. XPD was performed on the Cs  $4d$ , V  $2p$ , and Sb  $3d$  core levels, all of which show a pronounced XPD pattern with a sixfold symmetry.

The Cs  $4d$  pattern [Fig. 1(a)] recorded in the high-T phase shows an inner sixfold star (vertical orientation) surrounded by a ring of high intensity peaks in a straddled orientation (yellow circle). This is consistent with the pattern [Fig. 1(b)] calculated using a Bloch wave approach with the normal state crystal structure param-

eters determined by XRD [53, 54]. Below the CDW transition, the overall appearance of the XPD pattern does not change much [Fig. 1(c)], in agreement with the Bloch wave calculation considering the  $(2 \times 2 \times 4)$  reconstruction [53, 54] [Fig. 1(d)]. To highlight the broken mirror symmetry (chirality) of the low-T XPD pattern we plot the difference  $I(k_x, k_y) - I(-k_x, k_y)$  in Fig. 1(e). While the difference still shows a six-fold symmetry, the mirror symmetry of the XPD pattern is broken, as shown by a counterclockwise bending of the tips of the inner star in the XPD pattern. Indeed, a similar chirality shows up in the calculated XPD pattern [Fig. 1(f)] based on the low-T XRD data from Refs. [53, 54]. A corresponding analysis was performed for the V  $2p$  and Sb  $3d$  core level XPD patterns for  $T < T_{\text{CDW}}$  and  $T > T_{\text{CDW}}$  (see SM [51]). These results demonstrate the structural chirality of the CDW order and imply that the domain size is larger than the x-ray footprint on the sample ( $\approx 50 \mu\text{m}$  in diameter), consistent with earlier domain mapping studies [16].

To detect the chirality in the electronic structure valence band photoemission was performed. Circular dichroism experiments in the soft x-ray range were performed at the soft x-ray ARPES endstation of Beamline I09 at Diamond Light Source, UK [55]. The angle of incidence for the circularly polarized x-rays was  $\theta = 22.5^\circ$  with respect to the sample surface, which was oriented to align the  $\Gamma$ -M-L plane with the incident beam. The total energy resolution was set to 50 meV. Figure 2 shows the experimental Fermi surface of  $\text{CsV}_3\text{Sb}_5$  measured at the two temperatures  $T_H = 115$  K and  $T_L = 30$  K, *i.e.*, above and below  $T_{\text{CDW}} = 94$  K. In Figs. 2(a-e) we plot the photoemission intensity distribution  $I(E_F, k_x, k_y)$  at the Fermi energy as a function of the parallel momentum  $k_x, k_y$ . The photon energies were varied in an interval from 210 eV to 250 eV, covering a perpendicular momentum range from  $k_z = 11G_{001}$  to  $12G_{001}$  [Fig. 2(c-e)]. We observe no significant dispersion along  $k_z$ , indicating a two-dimensional character of the electronic states. This is in agreement with previous observations [2].

From the photoemission intensities measured with circularly polarized x-ray excitation,  $I^{+/-}$ , we determine the asymmetry  $A^* = (I^+ - I^-)/(I^+ + I^-)$ . The non-relativistic circular dichroism in the angular distribution (CDAD) is a geometric effect and it is strictly antisymmetric with respect to the photon plane of incidence, which coincides with the  $\Gamma$ -M-A crystal mirror plane [56]. To separate the CDAD from any other contribution, we calculate the asymmetry shown in Figs. 2(f-j) as  $A_{\text{CDAD}}(k_x, k_y) = (1/2)[A^*(k_x, k_y) - A^*(k_x, -k_y)]$  (see detailed discussion of the separation procedure in Ref. [57]). The maximum asymmetry is 0.5, and leads to a significant intensity redistribution when the x-ray helicity is switched. The CDAD asymmetry depends strongly on the photon energy, as can be seen by comparing Figs. 2(f) and 2(g) (see Ref. [58]). The photon energy series shows a continuous change of the asymme-

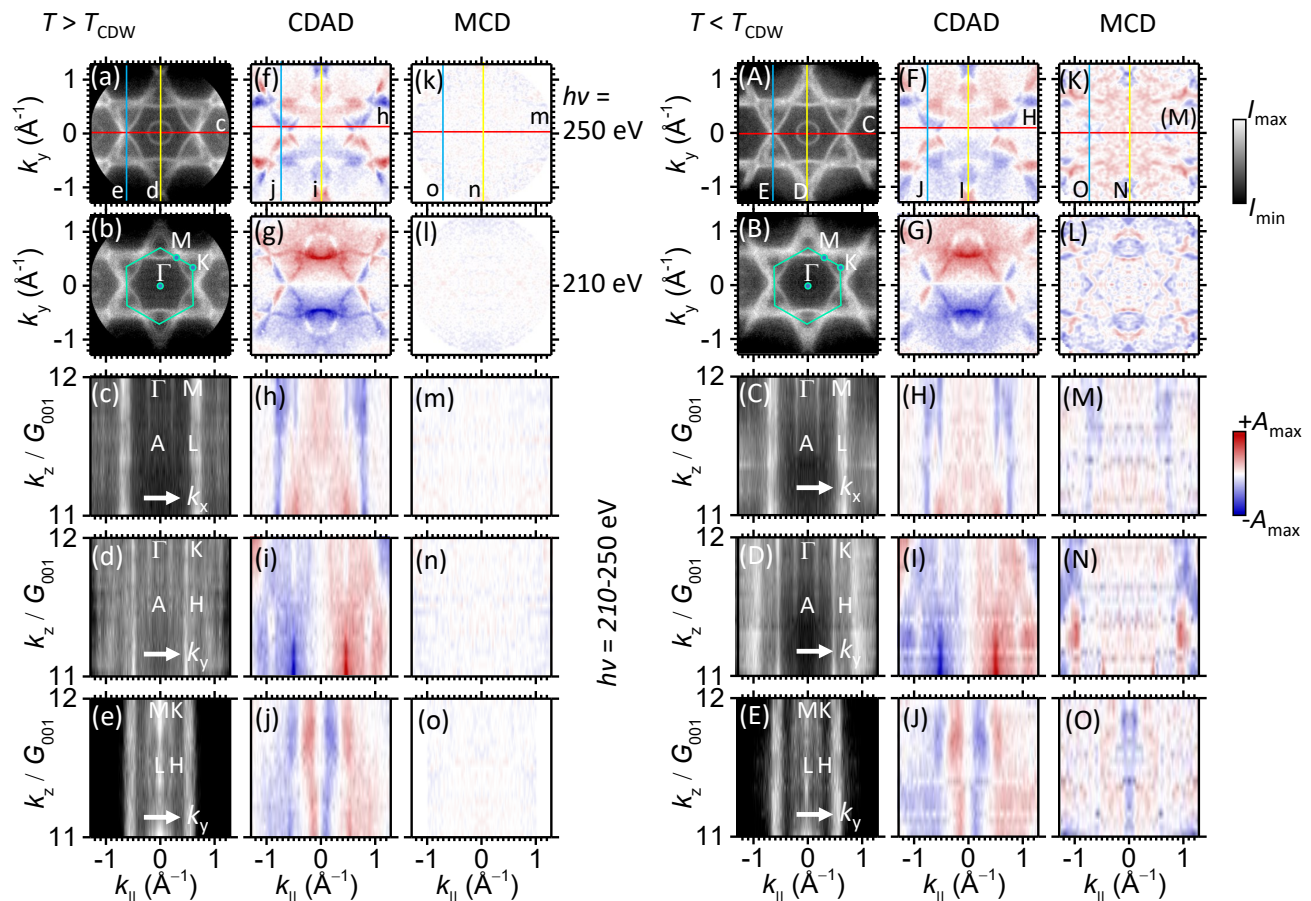


FIG. 2. (a,b) Fermi surface of  $\text{CsV}_3\text{Sb}_5$  measured at  $h\nu = 250$  eV (a) and 210 eV (b) for  $T > T_{\text{CDW}}$ . The photon incidence is from the right. (c-e) Fermi surface sections in the  $k_z - k_{\parallel}$  planes (perpendicular to the surface) corresponding to the lines indicated in (a). The photon energy has been varied between 210 and 250 eV in small steps. (f-j)  $A_{\text{CDAD}}$  in the same Fermi surface sections as in (a-e) [(h) shifted to  $k_y > 0$  to avoid the  $A_{\text{CDAD}} = 0$ -line]. The maximum asymmetry of the color scale (right) is  $A_{\text{max}} = 0.5$ . (k-o)  $A_{\text{MCD}}$  in the same Fermi surface sections as in (a-e). The maximum asymmetry of the color scale is in this case  $A_{\text{max}} = 0.1$ . (A-O) Similar data measured at 30 K ( $T < T_{\text{CDW}}$ ) plotted on the same scales.

try with varying  $k_z$  for several electronic bands. Only the states near the M-L-line show a constant asymmetry independent of the photon energy, as emphasized by the  $k_z$ -dependence shown in Figs. 2(h) and 2(j).

Note that at  $T > T_{\text{CDW}}$ , the dichroism is completely dominated by the CDAD. This can be visualized by the complementary magnetic circular dichroism (MCD), which is symmetric with respect to the  $k_y$  direction [59],  $A_{\text{MCD}}(k_x, k_y) = (1/2)[A^*(k_x, k_y) + A^*(k_x, -k_y)]$ , as shown in Figs. 2(k-o).  $A_{\text{MCD}}$  is less than 0.01 and shows no systematic variation as a function of parallel and perpendicular momentum. The lack of  $A_{\text{MCD}}$  confirms the non-magnetic character of the electronic states in  $\text{CsV}_3\text{Sb}_5$  in its normal state at  $T > T_{\text{CDW}}$ .

At 30 K, the average photoemission intensity distribution shown in Figs. 2(A-E) has not changed much. There are no obvious changes in the dispersion of the visible bands, only the intensity distribution near the M-L line [central line at  $k_{\parallel} = 0$  in Fig. 2(E)] changes

slightly. This observation is in agreement with previous reports using a higher energy resolution [60, 61], where the CDW-induced gap opening appears near the M-point. The CDW-induced band gap is discussed in the SM [51].

The CDAD asymmetry in the CDW state [Figs. 2(F-J)] shows a similar pattern to that observed in the normal state. The fact that no obvious CDW-induced change in CDAD is observed implies the absence of a significant change in orbital charge redistribution.

In contrast, the low-T data show a significant  $k_y$ -symmetric  $A_{\text{MCD}}$  [Figs. 2(K-O)]. A prominent, almost  $k_z$ -independent, contribution appears near the M-L line at  $(k_x = \pm 0.7 \text{ \AA}^{-1}, k_y = 0, k_z)$ . This is unexpected for a paramagnetic system. The two M-points at  $k_y = 0$  coincide with the antisymmetry axis of the CDAD, where the CDAD vanishes. The large asymmetry of about -0.1 is essentially independent of the photon energy [Figs. 2(M) and 2(O)]. Especially near  $k_y = 0$  a pronounced non-zero  $A_{\text{MCD}}$  occurs that cannot be explained by an artefact due

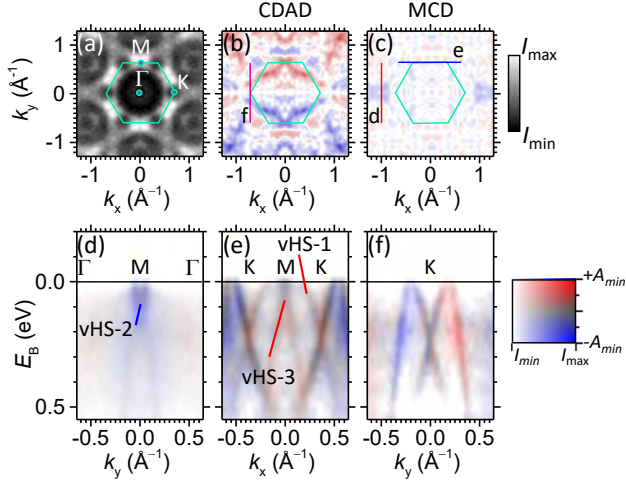


FIG. 3. (a) Fermi surface of  $\text{CsV}_3\text{Sb}_5$  measured at a photon energy of 330 eV for  $T < T_{\text{CDW}}$ . The photon incidence is from the right. (b) CDAD texture of the Fermi surface. The maximum asymmetry of the color scale (right) is  $A_{\text{max}} = 0.5$ . (c) MCD asymmetry of the Fermi surface. The maximum asymmetry of the color scale (right) is  $A_{\text{max}} = 0.1$ . (d,e) Band dispersion with overlaid MCD asymmetry (two-dimensional color scale on the right) along the indicated lines in (c). (f) Band dispersion with overlaid CDAD asymmetry across the K-point along the indicated line in (b).

to different sample illumination. Significant  $A_{\text{MCD}}$  values also show up at  $(k_x = 0, k_y = \pm 1 \text{ \AA}^{-1}, k_z)$  [Fig. 2(N)]. Here, the sign of  $A_{\text{MCD}}$  changes at about  $k_z = 11.5G_{001}$ , which hints to additional diffraction-related asymmetries or matrix-element effects [58].

Further details of the band dispersion versus binding energy as measured at 30 K and 115 K are discussed in SM [51].

To further elucidate the CDW-induced chirality using a different experimental geometry, we performed a soft x-ray photoemission experiment with the time-of-flight momentum microscope at the soft x-ray beamline P04 at PETRA III, DESY, Germany [62], with the total energy resolution set to 34 meV. We used 330 eV x-rays (corresponding to  $k_z = 13.7G_{001}$ ) and the same angle of incidence  $\theta = 22.5^\circ$ . In this case, however, the plane of incidence was along the  $\Gamma$ -K-H plane.

Figure 3(a) shows the measured Fermi surface recorded in this configuration at 30 K. The CDAD asymmetry at the Fermi surface, Fig. 3(b) is antisymmetric with respect to the plane of incidence, with the maximum asymmetry  $A_{\text{max}} \approx 0.5$  similar to the previous case. The MCD asymmetry Fig. 3(c) also shows negative values up to  $-0.1$  near the M-point at  $(k_x, k_y) = (\pm 1 \text{ \AA}^{-1}, 0)$  in the adjacent Brillouin zones on the  $\Gamma$ -K symmetry axis ( $k_y = 0$ -axis). The sections along M- $\Gamma$  [Fig. 3(d)] and M-K [Fig. 3(e)] suggest that the negative MCD asymmetry is related to the electron-like band with a maximum binding energy of 0.1 eV at the M-point, which belongs

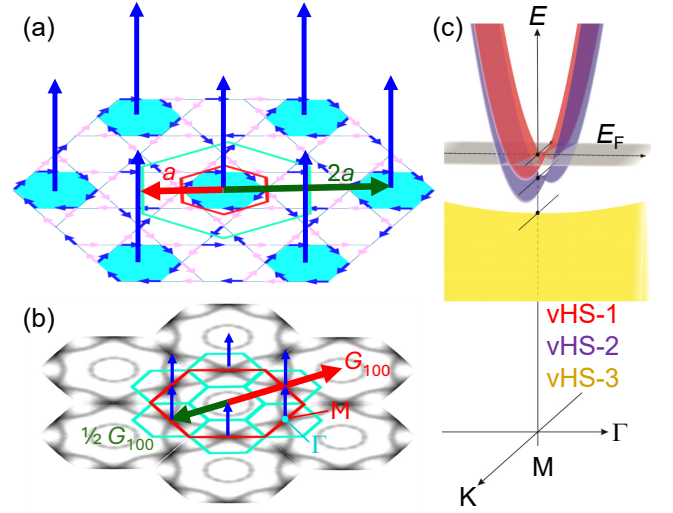


FIG. 4. (a) V-Sb plane constituting the kagome lattice. Small arrows indicate the loop current order forming a  $2 \times 2$  superstructure of orbital moments (large arrows). The superstructure Wigner-Seitz cell is indicated in green and the normal state unit cell in red with corresponding unit vectors along the  $a$ -axis. (b) Fermi surface in reciprocal space (grey level is proportional to the measured photoemission intensity). Hexagons indicate the Brillouin zones of the normal state structure (red) and the  $2 \times 2$  superstructure (green) with corresponding reciprocal lattice vectors. The blue arrows indicate the expected orbital moments near the M-points where the Fermi wave vector and the  $\Gamma$  points of the  $2 \times 2$  superstructure coincide. (c) Sketch of the first three vHSs near  $E_F$ .

to the van Hove singularity vHS-2 [see SM for a detailed description of the vHSs [51] and Fig. 4(c)]. Bands associated with vHS-1, *i.e.*, the flat band near the Fermi level at the M-point [see Fig. 3(e)], and vHS-3 (hole-like band) have positive  $A_{\text{MCD}}$  values. The large MCD asymmetries near the M-points confirm our findings obtained with the photon plane of incidence coinciding with the  $\Gamma$ -M-A plane [Fig. 2].

Since the multiple vHSs with opposite mirror eigenvalues are close in energy, it has been proposed that the nearest neighbor electron repulsion favors a ground state with coexisting loop current order and charge-bond order [63]. The loop current order imposes a time-reversal symmetry breaking in the CDW phase.

Figure 4(a) schematically shows the charge loop current as adapted from Ref. [2]. It can be visualized by alternating charge currents along the three sets of parallel lines connecting the V atom positions. Thus, the charge current vanishes when integrated over the unit cell. The ordered charge current along the V-V bonds leads to loop currents, [Fig. 4(a)], that bypass the six V atoms. The current direction of individual bonds can be either clockwise (blue arrows) or counterclockwise (pink arrows). Every second loop shows an unfrustrated loop current (shown in light blue) forming a  $2 \times 2$  superlattice.

In reciprocal space, the corresponding Brillouin zone of the  $2 \times 2$  structure is shown in green in Fig. 4(b). Here, some  $\Gamma$ -points of the superstructure Brillouin zone coincide with the M-points of the larger normal-state Brillouin zone [red in Fig. 4(b)]. Since the van Hove singularities near the Fermi surface are located at these M-points, states with finite orbital angular momentum causing a MCD are also expected at these coincidence points [blue arrows in Fig. 4(b)].

Our experimental results are thus consistent with recent reports on the anomalous Hall effect [32, 40–42], observations of chiral charge order in STM studies [31] and the early magneto-optical Kerr effect studies [16, 30, 32, 40–45], all suggesting an orbital loop-current-order. On the other hand, recent dedicated polar Kerr effect measurements seem to rule out the time-reversal symmetry breaking in  $\text{CsV}_3\text{Sb}_5$  [46, 48]. The absence of a measurable spontaneous Kerr effect (bulk probe) [48], with strong evidence for chiral charge ordering from surface sensitive techniques such as STM [31] and the presented ARPES data, may imply an antiferromagnetic interlayer ordering of the orbital magnetic moments in  $\text{CsV}_3\text{Sb}_5$ . In this case, optical dichroism averaged over many atomic layers would disappear.

On the other hand, our photoelectron diffraction results at 6 keV have shown have shown that the lattice exhibits a chiral structure in the CDW state, which is consistent with XRD data implying a stacking of different CDW patterns along the  $c$ -axis [53, 54]. The co-existence of the Star-of-David and inverse Star-of-David reconstructions in the CDW state is demonstrated by XRD [39, 64], nuclear quadrupole resonance (NQR) [65], and nuclear magnetic resonance (NMR) [66] measurements. Such structural chirality may also induce the observed valence-band MCD effect, which is in this case better described as an intrinsic instead of a magnetic circular dichroism [67]. In fact, a three-dimensional structural and electronic chirality of the helix-type without time-reversal symmetry breaking would also be consistent with our experimental results. The observed asymmetry values of the order of 0.1 are, however, much larger than previously assumed for the natural circular dichroism.

This work was funded by the Deutsche Forschungsgemeinschaft (DFG, German Research Foundation), grant no. TRR288–422213477 (projects B03, B04, and B08), and grant no Scho341/16-1, through the Collaborative Research Center SFB 1170 ToCoTronics (Project No. 258499086), through the Würzburg–Dresden Cluster of Excellence on Complexity and Topology in Quantum Matter ct.qmat (EXC 2147, Project No. 390858490), and by the BMBF (projects 05K22UM2, 05K22UM4, and 05K22WW1). Funding for the instrument by the Federal Ministry of Education and Research (BMBF) under framework program ErUM is gratefully acknowl-

edged. We thank the Diamond Light Source for providing beamtime at beamline I09. We acknowledge DESY (Hamburg, Germany) for the provision of experimental facilities. Parts of this research were carried out at PE-TRA III using beamlines P04 and P22.

---

\* elmers@uni-mainz.de

- [1] C. Guo, M. R. van Delft, M. Gutierrez-Amigo, D. Chen, C. Putzke, G. Wagner, M. H. Fischer, T. Neupert, I. Errea, M. G. Vergniory, S. Wiedmann, C. Felser, and P. J. W. Moll, *npj Quantum Materials* **9**, 20 (2024).
- [2] Y. Hu, X. Wu, A. P. Schnyder, and M. Shi, *npj Quantum Materials* **8**, 67 (2023).
- [3] M. Kang, S. Fang, J.-K. Kim, B. R. Ortiz, S. H. Ryu, J. Kim, J. Yoo, G. Sangiovanni, D. Di Sante, B.-G. Park, C. Jozwiak, A. Bostwick, E. Rotenberg, E. Kaxiras, S. D. Wilson, J.-H. Park, and R. Comin, *Nature Physics* **18**, 301 (2022).
- [4] M. Sato and Y. Ando, *Reports on Progress in Physics* **80**, 076501 (2017).
- [5] Y. Xing, S. Bae, E. Ritz, F. Yang, T. Birol, A. N. Capa Salinas, B. R. Ortiz, S. D. Wilson, Z. Wang, R. M. Fernandes, and V. Madhavan, *Nature* **631**, 60 (2024).
- [6] G. Xu, B. Lian, and S.-C. Zhang, *Physical Review Letters* **115**, 186802 (2015).
- [7] H.-M. Guo and M. Franz, *Physical Review B* **80**, 113102 (2009).
- [8] E. Tang, J.-W. Mei, and X.-G. Wen, *Physical Review Letters* **106**, 236802 (2011).
- [9] W.-S. Wang, Z.-Z. Li, Y.-Y. Xiang, and Q.-H. Wang, *Physical Review B* **87**, 115135 (2013).
- [10] M. L. Kiesel, C. Platt, and R. Thomale, *Physical Review Letters* **110**, 126405 (2013).
- [11] M. L. Kiesel and R. Thomale, *Physical Review B* **86**, 121105(R) (2012).
- [12] S.-L. Yu and J.-X. Li, *Physical Review B* **85**, 144402 (2012).
- [13] A. Mielke, *Journal of Physics A: Mathematical and General* **25**, 4335 (1992).
- [14] S. Vonsovsky and M. Katsnelson, *Physica B: Condensed Matter* **159**, 61 (1989).
- [15] M. Frachet, L. Wang, W. Xia, Y. Guo, M. He, N. Maraytta, R. Heid, A.-A. Haghighirad, M. Merz, C. Meingast, and F. Hardy, *Physical Review Letters* **132**, 186001 (2024).
- [16] Y. Xu, Z. Ni, Y. Liu, B. R. Ortiz, Q. Deng, S. D. Wilson, B. Yan, L. Balents, and L. Wu, *Nature Physics* **18**, 1470 (2022).
- [17] L. Nie, K. Sun, W. Ma, D. Song, L. Zheng, Z. Liang, P. Wu, F. Yu, J. Li, M. Shan, D. Zhao, S. Li, B. Kang, Z. Wu, Y. Zhou, K. Liu, Z. Xiang, J. Ying, Z. Wang, T. Wu, and X. Chen, *Nature* **604**, 59 (2022).
- [18] H. Zhao, H. Li, B. R. Ortiz, S. M. L. Teicher, T. Park, M. Ye, Z. Wang, L. Balents, S. D. Wilson, and I. Zeljkovic, *Nature* **599**, 216 (2021).
- [19] H. Li, T. Zhang, T. Yilmaz, Y. Pai, C. Marvinney, A. Said, Q. Yin, C. Gong, Z. Tu, E. Vescovo, C. Nelson, R. Moore, S. Murakami, H. Lei, H. Lee, B. Lawrie, and H. Miao, *Physical Review X* **11**, 031050 (2021).
- [20] Z. Liang, X. Hou, F. Zhang, W. Ma, P. Wu, Z. Zhang,

- F. Yu, J.-J. Ying, K. Jiang, L. Shan, Z. Wang, and X.-H. Chen, *Physical Review X* **11**, 031026 (2021).
- [21] H. Chen, H. Yang, B. Hu, Z. Zhao, J. Yuan, Y. Xing, G. Qian, Z. Huang, G. Li, Y. Ye, S. Ma, S. Ni, H. Zhang, Q. Yin, C. Gong, Z. Tu, H. Lei, H. Tan, S. Zhou, C. Shen, X. Dong, B. Yan, Z. Wang, and H.-J. Gao, *Nature* **599**, 222 (2021).
- [22] Z. Guguchia, C. Mielke, D. Das, R. Gupta, J.-X. Yin, H. Liu, Q. Yin, M. H. Christensen, Z. Tu, C. Gong, N. Shumiya, M. S. Hossain, T. Gamsakhurdashvili, M. Elender, P. Dai, A. Amato, Y. Shi, H. C. Lei, R. M. Fernandes, M. Z. Hasan, H. Luetkens, and R. Khasanov, *Nature Communications* **14**, 153 (2023).
- [23] K. Jiang, T. Wu, J.-X. Yin, Z. Wang, M. Z. Hasan, S. D. Wilson, X. Chen, and J. Hu, *National Science Review* **10**, nwac199 (2022).
- [24] Z. Zhang, Z. Chen, Y. Zhou, Y. Yuan, S. Wang, J. Wang, H. Yang, C. An, L. Zhang, X. Zhu, Y. Zhou, X. Chen, J. Zhou, and Z. Yang, *Physical Review B* **103**, 224513 (2021).
- [25] T. Neupert, M. M. Denner, J.-X. Yin, R. Thomale, and M. Z. Hasan, *Nature Physics* **18**, 137 (2021).
- [26] K. Chen, N. Wang, Q. Yin, Y. Gu, K. Jiang, Z. Tu, C. Gong, Y. Uwatoko, J. Sun, H. Lei, J. Hu, and J.-G. Cheng, *Physical Review Letters* **126**, 247001 (2021).
- [27] X. Chen, X. Zhan, X. Wang, J. Deng, X.-B. Liu, X. Chen, J.-G. Guo, and X. Chen, *Chinese Physics Letters* **38**, 057402 (2021).
- [28] H. Tan, Y. Liu, Z. Wang, and B. Yan, *Physical Review Letters* **127**, 046401 (2021).
- [29] B. R. Ortiz, S. M. Teicher, Y. Hu, J. L. Zuo, P. M. Sarte, E. C. Schueller, A. M. Abeykoon, M. J. Krogstad, S. Rosenkranz, R. Osborn, R. Seshadri, L. Balents, J. He, and S. D. Wilson, *Physical Review Letters* **125**, 247002 (2020).
- [30] C. Mielke, D. Das, J.-X. Yin, H. Liu, R. Gupta, Y.-X. Jiang, M. Medarde, X. Wu, H. C. Lei, J. Chang, P. Dai, Q. Si, H. Miao, R. Thomale, T. Neupert, Y. Shi, R. Khasanov, M. Z. Hasan, H. Luetkens, and Z. Guguchia, *Nature* **602**, 245 (2022).
- [31] Y.-X. Jiang, J.-X. Yin, M. M. Denner, N. Shumiya, B. R. Ortiz, G. Xu, Z. Guguchia, J. He, M. S. Hossain, X. Liu, J. Ruff, L. Kautzsch, S. S. Zhang, G. Chang, I. Belopolski, Q. Zhang, T. A. Cochran, D. Multer, M. Litskevich, Z.-J. Cheng, X. P. Yang, Z. Wang, R. Thomale, T. Neupert, S. D. Wilson, and M. Z. Hasan, *Nature Materials* **20**, 1353 (2021).
- [32] S.-Y. Yang, Y. Wang, B. R. Ortiz, D. Liu, J. Gayles, E. Derunova, R. Gonzalez-Hernandez, L. Šmejkal, Y. Chen, S. S. P. Parkin, S. D. Wilson, E. S. Toberer, T. McQueen, and M. N. Ali, *Science Advances* **6**, eabb6003 (2020).
- [33] Y. Hu, S. M. Teicher, B. R. Ortiz, Y. Luo, S. Peng, L. Huai, J. Ma, N. C. Plumb, S. D. Wilson, J. He, and M. Shi, *Science Bulletin* **67**, 495 (2022).
- [34] Y.-P. Lin and R. M. Nandkishore, *Physical Review B* **104**, 045122 (2021).
- [35] T. Park, M. Ye, and L. Balents, *Physical Review B* **104**, 035142 (2021).
- [36] X. Feng, K. Jiang, Z. Wang, and J. Hu, *Science Bulletin* **66**, 1384 (2021).
- [37] X. Wu, T. Schwemmer, T. Müller, A. Consiglio, G. Sangiovanni, D. Di Sante, Y. Iqbal, W. Hanke, A. P. Schnyder, M. M. Denner, M. H. Fischer, T. Neupert, and R. Thomale, *Physical Review Letters* **127**, 177001 (2021).
- [38] M. M. Denner, R. Thomale, and T. Neupert, *Physical Review Letters* **127**, 217601 (2021).
- [39] B. R. Ortiz, P. M. Sarte, E. M. Kenney, M. J. Graf, S. M. L. Teicher, R. Seshadri, and S. D. Wilson, *Physical Review Materials* **5**, 034801 (2021).
- [40] X. Wei, C. Tian, H. Cui, Y. Zhai, Y. Li, S. Liu, Y. Song, Y. Feng, M. Huang, Z. Wang, Y. Liu, Q. Xiong, Y. Yao, X. C. Xie, and J.-H. Chen, *Nature Communications* **15**, 5038 (2024).
- [41] X. Zhou, H. Liu, W. Wu, K. Jiang, Y. Shi, Z. Li, Y. Sui, J. Hu, and J. Luo, *Physical Review B* **105**, 205104 (2022).
- [42] F. H. Yu, T. Wu, Z. Y. Wang, B. Lei, W. Z. Zhuo, J. J. Ying, and X. H. Chen, *Physical Review B* **104**, L041103 (2021).
- [43] R. Khasanov, D. Das, R. Gupta, C. Mielke, M. Elender, Q. Yin, Z. Tu, C. Gong, H. Lei, E. T. Ritz, R. M. Fernandes, T. Birol, Z. Guguchia, and H. Luetkens, *Physical Review Research* **4**, 023244 (2022).
- [44] Y. Hu, S. Yamane, G. Mattoni, K. Yada, K. Obata, Y. Li, Y. Yao, Z. Wang, J. Wang, C. Farhang, J. Xia, Y. Maeno, and S. Yonezawa, “Time-reversal symmetry breaking in charge density wave of  $\text{CsV}_3\text{Sb}_5$  detected by polar kerr effect,” arXiv:2208.08036v2 (2022).
- [45] Q. Wu, Z. X. Wang, Q. M. Liu, R. S. Li, S. X. Xu, Q. W. Yin, C. S. Gong, Z. J. Tu, H. C. Lei, T. Dong, and N. L. Wang, *Physical Review B* **106**, 205109 (2022).
- [46] C. Farhang, J. Wang, B. R. Ortiz, S. D. Wilson, and J. Xia, *Nature Communications* **14**, 5326 (2023).
- [47] J. Wang, C. Farhang, B. R. Ortiz, S. D. Wilson, and J. Xia, *Physical Review Materials* **8**, 014202 (2024).
- [48] D. R. Saykin, C. Farhang, E. D. Kountz, D. Chen, B. R. Ortiz, C. Shekhar, C. Felser, S. D. Wilson, R. Thomale, J. Xia, and A. Kapitulnik, *Physical Review Letters* **131**, 016901 (2023).
- [49] H. Li, S. Wan, H. Li, Q. Li, Q. Gu, H. Yang, Y. Li, Z. Wang, Y. Yao, and H.-H. Wen, *Physical Review B* **105**, 045102 (2022).
- [50] F. Stier, A. A. Haghighirad, G. Garbarino, S. Mishra, N. Stölkerich, D. Chen, C. Shekhar, T. Laczmann, C. Felser, T. Ritschel, J. Geck, and M. L. Tacon, “Pressure-dependent electronic superlattice in the kagome-superconductor  $\text{CsV}_3\text{Sb}_5$ ,” arXiv:2404.14790v1 (2024).
- [51] “See Supplemental material at [URL will be inserted by publisher] for additional XPD data on V 2p and Sb 3d core levels, details on the electronic band dispersion and the discussion of CDW induced changes in the electronic structure near the M point of  $\text{CsV}_3\text{Sb}_5$ .”
- [52] C. Schlueter, A. Gloskovskii, K. Ederer, I. Schostak, S. Piec, I. Sarkar, Y. Matveyev, P. Lömker, M. Sing, R. Claessen, C. Wiemann, C. M. Schneider, K. Medjanik, G. Schönhense, P. Amann, A. Nilsson, and W. Drube, in *AIP Conference Proceedings*, Vol. 2054 (AIP, 2019) p. 040010.
- [53] L. Kautzsch, B. R. Ortiz, K. Mallayya, J. Plumb, G. Pokharel, J. P. C. Ruff, Z. Islam, E.-A. Kim, R. Seshadri, and S. D. Wilson, *Physical Review Materials* **7**, 024806 (2023).
- [54] B. R. Ortiz, S. M. Teicher, L. Kautzsch, P. M. Sarte, N. Ratcliff, J. Harter, J. P. Ruff, R. Seshadri, and S. D. Wilson, *Physical Review X* **11**, 041030 (2021).
- [55] M. Schmitt, D. Biswas, O. Tkach, O. Fedchenko, J. Liu,

- H.-J. Elmers, M. Sing, R. Claessen, T.-L. Lee, and G. Schönhense, “Hybrid photoelectron momentum microscope at the soft x-ray beamline i09 of the diamond light source,” arXiv:2406.00771v1 (2024).
- [56] C. Westphal, J. Bansmann, M. Getzlaff, and G. Schönhense, *Physical Review Letters* **63**, 151 (1989).
- [57] O. Fedchenko, J. Minár, A. Akashdeep, S. W. D’Souza, D. Vasilyev, O. Tkach, L. Odenbreit, Q. Nguyen, D. Kutnyakhov, N. Wind, L. Wenthaus, M. Scholz, K. Rossnagel, M. Hoesch, M. Aeschlimann, B. Stadtmüller, M. Kläui, G. Schönhense, T. Jungwirth, A. B. Hellenes, G. Jakob, L. Šmejkal, J. Sinova, and H.-J. Elmers, *Science Advances* **10**, eadj4883 (2024).
- [58] O. Fedchenko, K. Medjanik, S. Chernov, D. Kutnyakhov, M. Ellguth, A. Oelsner, B. Schönhense, T. R. F. Peixoto, P. Lutz, C.-H. Min, F. Reinert, S. Däster, Y. Acremann, J. Viefhaus, W. Wurth, J. Braun, J. Minár, H. Ebert, H. J. Elmers, and G. Schönhense, *New Journal of Physics* **21**, 013017 (2019).
- [59] J. Bansmann, C. Westphal, M. Getzlaff, F. Fegél, and G. Schönhense, *Journal of Magnetism and Magnetic Materials* **104-107**, 1691 (1992).
- [60] K. Nakayama, Y. Li, T. Kato, M. Liu, Z. Wang, T. Takahashi, Y. Yao, and T. Sato, *Phys. Rev. B* **104**, L161112 (2021).
- [61] D. Azoury, A. von Hoegen, Y. Su, K. H. Oh, T. Holder, H. Tan, B. R. Ortiz, A. Capa Salinas, S. D. Wilson, B. Yan, and N. Gedik, *Proceedings of the National Academy of Sciences* **120**, e2308588120 (2023).
- [62] O. Tkach, S. Fragkos, Q. Nguyen, S. Chernov, M. Scholz, N. Wind, S. Babenkov, O. Fedchenko, Y. Lytvynenko, D. Zimmer, A. Hloskovskii, D. Kutnyakhov, F. Pressacco, J. Dilling, L. Bruckmeier, M. Heber, F. Scholz, J. Sobota, J. Koralek, N. Sirica, M. Kallmayer, M. Hoesch, C. Schlueter, L. V. Odnodvoretz, Y. Mairesse, K. Rossnagel, H. J. Elmers, S. Beaulieu, and G. Schoenhense, “Multi-mode front lens for momentum microscopy: Part ii experiments,” arXiv:2401.10084v2 (2024).
- [63] H. Li, Y. B. Kim, and H.-Y. Kee, *Physical Review Letters* **132**, 146501 (2024).
- [64] Q. Xiao, Y. Lin, Q. Li, X. Zheng, S. Francoual, C. Plueckthun, W. Xia, Q. Qiu, S. Zhang, Y. Guo, J. Feng, and Y. Peng, *Physical Review Research* **5**, L012032 (2023).
- [65] X. Y. Feng, Z. Zhao, J. Luo, J. Yang, A. F. Fang, H. T. Yang, H. J. Gao, R. Zhou, and G.-q. Zheng, *npj Quantum Materials* **8**, 23 (2023).
- [66] J. Frassinetti, P. Bonfà, G. Allodi, E. Garcia, R. Cong, B. R. Ortiz, S. D. Wilson, R. De Renzi, V. F. Mitrović, and S. Sanna, *Physical Review Research* **5**, L012017 (2023).
- [67] S. S. Brinkman, X. L. Tan, B. Brekke, A. C. Mathisen, O. Finnseth, R. J. Schenk, K. Hagiwara, M.-J. Huang, J. Buck, M. Kallane, M. Hoesch, K. Rossnagel, K.-H. Ou Yang, M.-T. Lin, G.-J. Shu, Y.-J. Chen, C. Tusche, and H. Bentmann, *Physical Review Letters* **132**, 196402 (2024).

## Supplemental Material: Chirality in the Kagome Metal $\text{CsV}_3\text{Sb}_5$

H.J. Elmers,<sup>1,\*</sup> O. Tkach,<sup>1,2</sup> Y. Lytvynenko,<sup>1,3</sup> P. Yogi,<sup>1</sup> M. Schmitt,<sup>4,5</sup> D. Biswas,<sup>4</sup> J. Liu,<sup>4</sup> S. V. Chernov,<sup>6</sup> M. Hoesch,<sup>6</sup> D. Kutnyakhov,<sup>6</sup> N. Wind,<sup>6,7</sup> L. Wenthaus,<sup>6</sup> M. Scholz,<sup>6</sup> K. Rossnagel,<sup>7,8</sup> A. Gloskovskii,<sup>6</sup> C. Schlueter,<sup>6</sup> A. Winkelmann,<sup>9</sup> A.-A. Haghighirad,<sup>10</sup> T.-L. Lee,<sup>4</sup> M. Sing,<sup>5</sup> R. Claessen,<sup>5</sup> M. Le Tacon,<sup>10</sup> J. Demsar,<sup>1</sup> G. Schönhense,<sup>1</sup> and O. Fedchenko<sup>1</sup>

<sup>1</sup>*Institut für Physik, Johannes Gutenberg-Universität, Staudingerweg 7, D-55128 Mainz, Germany*

<sup>2</sup>*Sumy State University, Kharkivska 116, 40007 Sumy, Ukraine*

<sup>3</sup>*Institute of Magnetism of the NAS and MES of Ukraine, 03142 Kyiv, Ukraine*

<sup>4</sup>*Diamond Light Source Ltd., Didcot OX11 0DE, United Kingdom*

<sup>5</sup>*Physikalisches Institut and Würzburg-Dresden Cluster of Excellence ct.qmat, Julius-Maximilians-Universität, D-97074 Würzburg, Germany*

<sup>6</sup>*Deutsches Elektronen-Synchrotron DESY, 22607 Hamburg, Germany*

<sup>7</sup>*Institut für Experimentelle und Angewandte Physik, Christian-Albrechts-Universität zu Kiel, 24098 Kiel, Germany*

<sup>8</sup>*Ruprecht Haensel Laboratory, Deutsches Elektronen-Synchrotron DESY, 22607 Hamburg, Germany*

<sup>9</sup>*Academic Centre for Materials and Nanotechnology, AGH University of Krakow, 30059 Kraków, Poland*

<sup>10</sup>*Institute for Quantum Materials and Technologies, Karlsruhe Institute of Technology, 76021 Karlsruhe, Germany*

(Dated: August 8, 2024)

### EXPERIMENTAL

The hexagonal  $\text{CsV}_3\text{Sb}_5$  structure and the experimental geometries for the photoemission experiments are shown in Figs. 1(a) and 1(b), respectively.  $\text{CsV}_3\text{Sb}_5$  consists of a planar arrangement of V atoms forming a kagome lattice consisting of three sets of parallel lines of V atoms (red) with Sb atoms (gray) as nearest neighbors. The V-Sb planes are separated by Cs atoms, thus forming an electronically two-dimensional lattice.

The single crystals were freshly cleaved in ultrahigh vacuum. Circular dichroism experiments in the soft x-ray range were performed at the soft x-ray ARPES endstation of Beamline I09 at Diamond Light Source, UK [1]. The angle of incidence for the circularly polarized x-rays was  $\theta = 22.5^\circ$  with respect to the sample surface, which was oriented to align the  $\Gamma$ -M-L plane with the incident beam [see Fig. 1(b)]. In this case, the total energy resolution was set to 50 meV.

In addition, soft x-ray photoemission experiments with the time-of-flight momentum microscope at the soft x-ray beamline P04 at PETRA III, DESY, Germany [2], were performed with the total energy resolution set to 34 meV. We used 330 eV x-rays (corresponding to  $k_z = 13.7G_{001}$ ) and the same angle of incidence  $\theta = 22.5^\circ$ . In this case, however, the plane of incidence was along the  $\Gamma$ -K-H plane [see Fig. 1(b)].

We used throughout this article the Brillouin zone definition of the high temperature phase  $T > T_{\text{CDW}}$  as shown in Fig. 1(c).

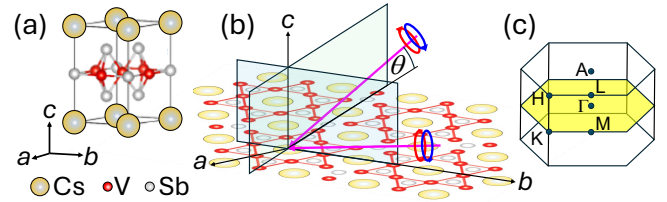


FIG. 1. (a) Hexagonal unit cell of  $\text{CsV}_3\text{Sb}_5$  in the normal state with unit vectors  $a$ ,  $b$ , and  $c$ . The angle between  $a$  and  $b$  is  $60^\circ$ . (b) Experimental geometry. The circularly polarized x-rays impinge on the (001) surface at an angle  $\theta$  within the  $b$ - $c$  plane or  $90^\circ$  rotated. (c) Brillouin zone of  $\text{CsV}_3\text{Sb}_5$  in the high temperature phase with marked high-symmetry points. The high-temperature phase notation was used throughout the paper.

### X-RAY PHOTOELECTRON DIFFRACTION (XPD)

Figure 2 shows experimental and calculated XPD patterns for all three core levels. All core levels show a pronounced XPD pattern with a sixfold symmetry. The Cs  $4d$  pattern [Fig. 2(a)] shows an inner sixfold star in a vertical orientation and an outer ring of high intensity peaks in a straddled orientation (circle). This is in agreement with the pattern calculated using a Bloch wave approach on an XRD-determined crystal structure in the normal state of  $\text{CsV}_3\text{Sb}_5$  [Fig. 2(b)]. Below the CDW transition, the inner star has a lower intensity [Fig. 2(g)], in agreement with the Bloch wave calculation for the  $(2 \times 2 \times 4)$  CDW reconstruction [Fig. 2(h)] (Structural data from Ref. [3, 4]). To highlight the broken mirror symmetry



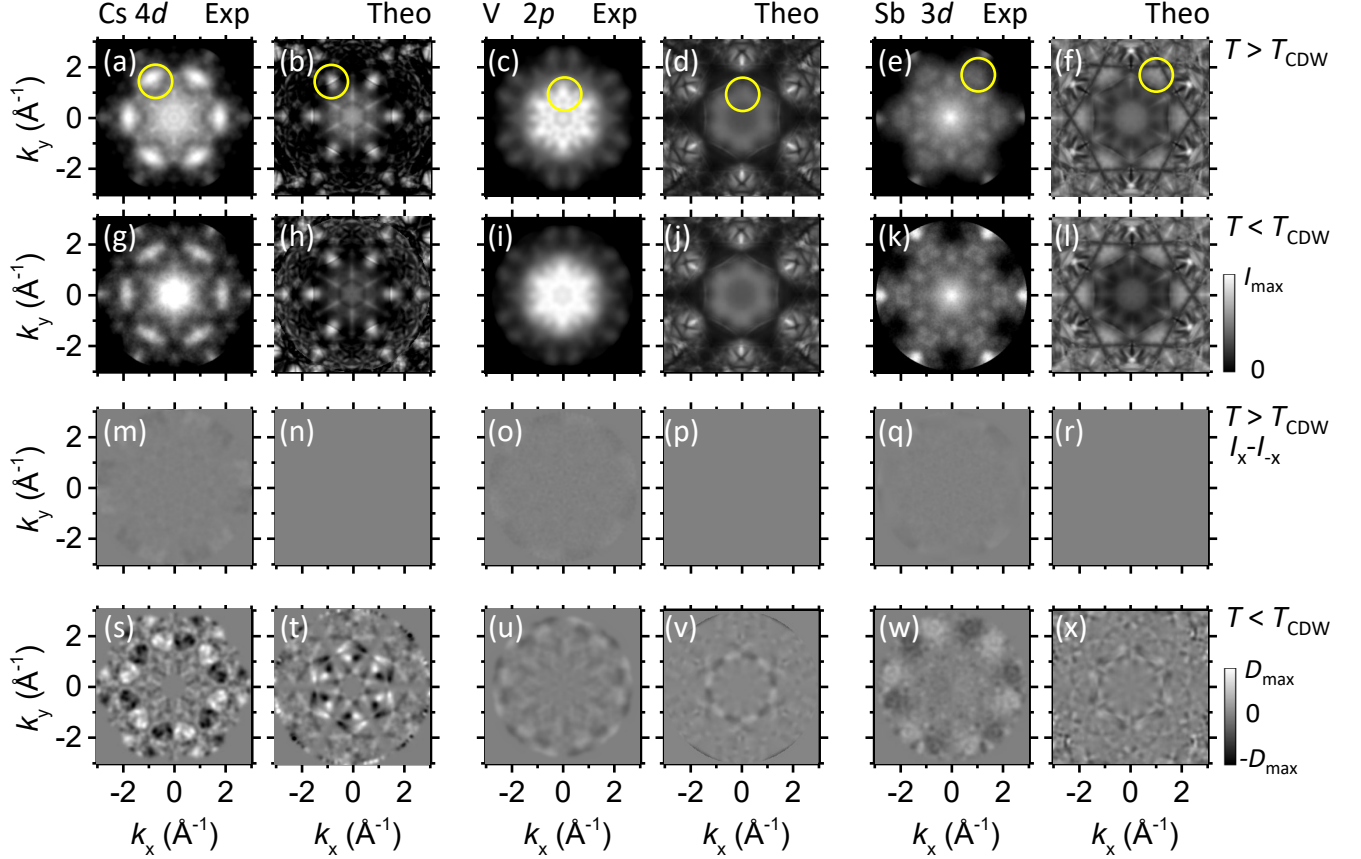


FIG. 2. X-ray photoelectron diffraction of  $\text{CsV}_3\text{Sb}_5$  measured at a photon energy of 6 keV and for  $T > T_{\text{CDW}}$  (first row) and  $T < T_{\text{CDW}}$  (second row), respectively. Comparison of experimental (a,c,e,g,i,k) and theoretical (b,d,f,h,j,l) data. Yellow circles highlight identical positions of theoretical and experimental data. (m,o,q,s,u,w) Difference of original data from (a,c,e,g,i,k) and data mirrored at  $k_x = 0$  to emphasize the broken mirror symmetry. (n,p,r,t,v,x) Similar data for the calculated results. The photoemission intensity is normalized to the maximum intensity  $I_{\text{max}}$  in each image. For the color scale  $D_{\text{max}}$  is set to 0.04.

(chirality) of the XPD pattern, we plot the difference  $I(k_x, k_y) - I(-k_x, k_y)$  in Fig. 2(m,s). For 115 K the difference is zero within error limits, indicating mirror symmetry. For 30 K, the difference also shows a six-fold symmetry. However, the mirror symmetry of the pattern is broken. A detailed inspection of the measured XPD pattern in Fig. 2(g) at 30 K shows that this symmetry breaking originates from a counterclockwise bending of the tips of the inner star and a corresponding lower intensity on the clockwise side of the tip. A similar symmetry breaking also shows up in the calculated pattern shown in Fig. 2(t). The mirror symmetric structure for  $T > T_{\text{CDW}}$  results in a mirror symmetric diffraction pattern as shown in Fig. 2(n).

A similar analysis was performed for the V  $2p$  and Sb  $3d$  XPD patterns. In the case of V  $2p$  [Fig. 2(c,i,d,j)] and Sb  $3d$  [Fig. 2(e,f,k,l)] the difference between  $T_L = 30$  K and  $T_H = 115$  K is very small for both experimental and theoretical data. For the Sb  $3d$  XPD patterns, we

observe a similarly reduced central intensity for  $T_L$  as compared to  $T_H$  as in the case of Cs  $4d$ . The difference images reveal that all low temperature patterns are chiral [Fig. 2(s,u,w)] in agreement with calculations [Fig. 2(t,v,x)] With values up to 0.04. The differences are significantly smaller for V  $2p$  and Sb  $3d$ , see grey level bar. Since the structural changes only affect the V and partly the Sb atomic positions, the scattering rather than the emitter atoms determine the diffraction patterns. A difference in the actual and assumed atomic positions could explain the remaining differences between experiment and theory.

#### DETAILS OF THE ELECTRONIC BAND DISPERSIONS

Figure 3 shows the Fermi surface and the band dispersion with an energy resolution of 50 meV, measured at 30 K and 115 K. The high (low) temperature data were

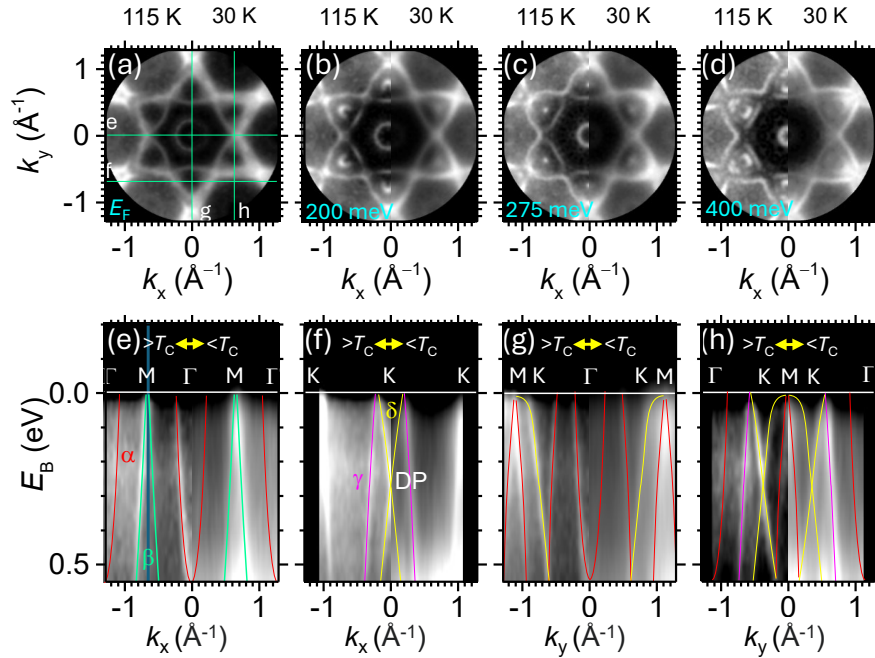


FIG. 3. (a-d) Temperature dependence of band dispersion. Constant energy sections of the photoemission intensities in the  $k_x - k_y$  plane at the indicated binding energies, measured at a photon energy of 250 (210) eV. (e-h) Band dispersions along the indicated high symmetry directions in reciprocal space. Data on the left of each panel are measured for  $T > T_{CDW}$  (250 eV) and on the right for  $T < T_{CDW}$  (210 eV).

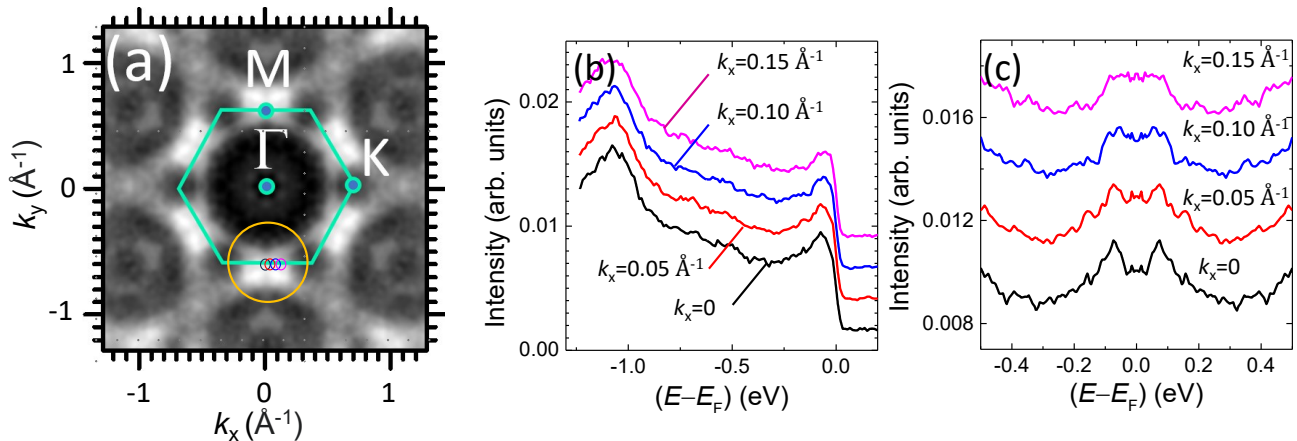


FIG. 4. (a) Fermi surface of  $\text{CsV}_3\text{Sb}_5$  from Fig. 4(a) of the main text. Colored circles in the center of the larger yellow circle near the M-point mark positions for the EDCs. (b) EDCs for distinct  $k_x$  values indicated in (a) along the M-K direction with  $k_x = 0$  denoting the M-point. (c) Sum of the EDCs from (b) and the same EDCs mirrored at the Fermi energy. The minimum at the Fermi level indicates the energy gap at the M-point.

measured at a photon energy of 250 eV (210 eV), where both photon energies correspond to an integer perpendicular reciprocal lattice vector.

In agreement with the theory and previous ARPES measurements we can identify the main band features. The sections across the  $\Gamma$ -K-M directions [Fig. 3(g,h)] show the van Hove singularities (vHSs) at the M-point

near the Fermi energy, which have a saddle point nature. vHS-1 is indicated by the flat yellow  $\delta$ -band at the M-point in Fig. 3(g,h). Along the perpendicular direction across the M-point Fig. 3(e), it is connected to an electron-like parabola, which is unoccupied at the M-point but acquires a higher binding energy towards the K-point. At the K-point the band marked by the yellow

line forms a Dirac cone with a Dirac point (DP) at a binding energy of 275 meV. This is shown in Figs. 3(c,f,h). vHS-2 is formed by the  $\alpha$ -band at the M-point (marked by the red line) with larger dispersion. In the perpendicular  $\Gamma$ -M direction [Fig. 3(e)] it forms an electron-like parabola with a maximum binding energy of less than 100 meV. vHS-3 at the M-point is connected to the lower Dirac cone at the K-point. It is outside the measured energy range. vHS-4 is related to the  $\beta$ -band (marked by the green line) [Fig. 3(e)] with the vHS located above the Fermi level. In the orthogonal direction but away from the M-point, this band deforms into the  $\gamma$ -band (marked by the purple line) shown in Fig. 3(f). Thus, vHS-1 and vHS-2 exhibit an electron-like state along the M-K direction and a hole-like state along the orthogonal M- $\Gamma$  direction and vice versa in the case of vHS-3 and vHS-4 [5–7].

The flat dispersion of vHS-1 (yellow-marked  $\delta$ -band in Fig. 3(h)) extends over more than half of the K-M path and indicates a higher-order nature of this van Hove singularity [5–7].

From the polarization-dependent ARPES measurements reported in Ref. [8] the orbital character of the states forming the van Hove singularities could be identified. The flat band of vHS-1 (yellow-marked  $\delta$ -band) was assigned to V  $d_{x^2-y^2}/d_{z^2}$  orbitals. vHS-2 is formed by  $d_{yz}$ -orbitals and vHS-3 by  $d_{xy}$ -orbitals. These van Hove singularities are related to the mirror-invariant V sublattice [6]. The Bloch states associated with vHS-1, vHS-2 and vHS-3 at the M point are characterized by  $A_g$ ,  $B_{2g}$  and  $B_{1g}$  irreducible representations with inversion-even parity. In contrast, vHS-4 corresponds to the  $B_{1u}$  irreducible representation, which is inversion-odd. vHS-4 arises from two sublattices, corresponding to a sublattice-mixed type of van Hove singularity [6, 7, 9], which is characterized by eigenstates that are evenly distributed over two of the three sublattices for each M-point.

At temperatures below  $T_{CDW}$  the CDW in CsV<sub>3</sub>Sb<sub>5</sub> leads to a reconstruction of the electronic structure as has been observed by ARPES [7, 10–12]. The in-plane  $2 \times 2$  modulation results in the folding of the pristine Brillouin zone [see Fig. 1(c) of the main text]. The CDW-induced band folding has been observed as an electron-like band around the  $\Gamma$ -point that has been back-folded from the M-point [13, 14]. In our case, the intensity near the  $\Gamma$ -point of the  $\alpha$ -band is already very low at 210 eV and there is no intensity inside the ring around  $\Gamma$ . In contrast, we observe the band gap associated with the in-plane CDW modulation along the  $\Gamma$ -K direction [Fig. 3(f,h)], which is consistent with previous experimental [10] and theoretical [15] results.

The band reconstructions in the ring near the  $\Gamma$ -point, caused by a hybridization of the Sb  $p$ -orbitals and the V  $d$ -orbitals, are not visible. On the other hand, the triangular constant-energy contours around the K-point seem to expand in the CDW phase [Fig. 3(b)] as observed

previously. Presumably, the shift of the vHS bands contributing to the band reconstructions is too small to be identified with the energy resolution of this experiment. This is also true for the  $(2 \times 2 \times 4)$  CDW reconstruction expected from previous work [7, 10].

It has been pointed out that CDW-induced band reconstructions observed by ARPES [7, 10] may be influenced by the sample preparation and precise composition. However, the coexistence of the Star-of-David and inverse Star-of-David reconstructions in the CDW state is demonstrated by XRD [16, 17], nuclear quadrupole resonance (NQR) [18], and nuclear magnetic resonance (NMR) [19] measurements.

## ENERGY GAPS

Energy distribution curves (EDCs) at the M-point and along the M-K direction at  $k_x = 0.05, 0.1$ , and  $0.15 \text{ \AA}^{-1}$  show a systematic variation of the maximum intensity at or slightly below  $E_F$  [Fig. 4(b)]. To emphasize these changes, we plot the EDCs symmetrized at the Fermi level [Fig. 4(c)] as described in Ref. [14]. In this case, an energy gap appears as an intensity minimum at  $E_F$  framed by two intensity maxima. Indeed, we observe an energy gap of 80 meV in the close vicinity of the M-point, which closes at a larger distance from the M-point (c). This observation is in good agreement with previously reported results [8, 14].

---

\* elmers@uni-mainz.de

- [1] M. Schmitt, D. Biswas, O. Tkach, O. Fedchenko, J. Liu, H.-J. Elmers, M. Sing, R. Claessen, T.-L. Lee, and G. Schönhense, “Hybrid photoelectron momentum microscope at the soft x-ray beamline i09 of the diamond light source,” arXiv:2406.00771v1 (2024).
- [2] O. Tkach, S. Fragkos, Q. Nguyen, S. Chernov, M. Scholz, N. Wind, S. Babenkov, O. Fedchenko, Y. Lytvynenko, D. Zimmer, A. Hloskovskii, D. Kutnyakhov, F. Pressacco, J. Dilling, L. Bruckmeier, M. Heber, F. Scholz, J. Sobota, J. Koralek, N. Sirica, M. Kallmayer, M. Hoesch, C. Schlueter, L. V. Odnodvoret, Y. Mairesse, K. Rossnagel, H. J. Elmers, S. Beaulieu, and G. Schoenhense, “Multi-mode front lens for momentum microscopy: Part ii experiments,” arXiv:2401.10084v2 (2024).
- [3] L. Kautzsch, B. R. Ortiz, K. Mallayya, J. Plumb, G. Pokharel, J. P. C. Ruff, Z. Islam, E.-A. Kim, R. Seshadri, and S. D. Wilson, *Physical Review Materials* **7**, 024806 (2023).
- [4] B. R. Ortiz, S. M. Teicher, L. Kautzsch, P. M. Sarte, N. Ratcliff, J. Harter, J. P. Ruff, R. Seshadri, and S. D. Wilson, *Physical Review X* **11**, 041030 (2021).
- [5] W. Wu, Z. Shi, M. Ozerov, Y. Du, Y. Wang, X.-S. Ni, X. Meng, X. Jiang, G. Wang, C. Hao, X. Wang, P. Zhang, C. Pan, H. Pan, Z. Sun, R. Yang, Y. Xu, Y. Hou, Z. Yan,

- C. Zhang, H.-Z. Lu, J. Chu, and X. Yuan, *Nature Communications* **15**, 2313 (2024).
- [6] Y. Hu, X. Wu, B. R. Ortiz, S. Ju, X. Han, J. Ma, N. C. Plumb, M. Radovic, R. Thomale, S. D. Wilson, A. P. Schnyder, and M. Shi, *Nature Communications* **13**, 2220 (2022).
- [7] M. Kang, S. Fang, J.-K. Kim, B. R. Ortiz, S. H. Ryu, J. Kim, J. Yoo, G. Sangiovanni, D. Di Sante, B.-G. Park, C. Jozwiak, A. Bostwick, E. Rotenberg, E. Kaxiras, S. D. Wilson, J.-H. Park, and R. Comin, *Nature Physics* **18**, 301 (2022).
- [8] Y. Hu, X. Wu, A. P. Schnyder, and M. Shi, *npj Quantum Materials* **8**, 67 (2023).
- [9] X. Wu, T. Schwemmer, T. Müller, A. Consiglio, G. Sangiovanni, D. Di Sante, Y. Iqbal, W. Hanke, A. P. Schnyder, M. M. Denner, M. H. Fischer, T. Neupert, and R. Thomale, *Physical Review Letters* **127**, 177001 (2021).
- [10] Y. Hu, X. Wu, B. R. Ortiz, X. Han, N. C. Plumb, S. D. Wilson, A. P. Schnyder, and M. Shi, *Physical Review B* **106**, 1241106 (2022).
- [11] Y. Luo, S. Peng, S. M. L. Teicher, L. Huai, Y. Hu, Y. Han, B. R. Ortiz, Z. Liang, Z. Wei, J. Shen, Z. Ou, B. Wang, Y. Miao, M. Guo, M. Hashimoto, D. Lu, Z. Qiao, Z. Wang, S. D. Wilson, X. Chen, and J. He, *Physical Review B* **105**, 1241111 (2022).
- [12] R. Lou, A. Fedorov, Q. Yin, A. Kuibarov, Z. Tu, C. Gong, E. F. Schwier, B. Büchner, H. Lei, and S. Borisenko, *Physical Review Letters* **128**, 036402 (2022).
- [13] Z. Jiang, H. Ma, W. Xia, Z. Liu, Q. Xiao, Z. Liu, Y. Yang, J. Ding, Z. Huang, J. Liu, Y. Qiao, J. Liu, Y. Peng, S. Cho, Y. Guo, J. Liu, and D. Shen, *Nano Letters* **23**, 5625 (2023).
- [14] H. Luo, Q. Gao, H. Liu, Y. Gu, D. Wu, C. Yi, J. Jia, S. Wu, X. Luo, Y. Xu, L. Zhao, Q. Wang, H. Mao, G. Liu, Z. Zhu, Y. Shi, K. Jiang, J. Hu, Z. Xu, and X. J. Zhou, *Nature Communications* **13**, 273 (2022).
- [15] C. Mielke, D. Das, J.-X. Yin, H. Liu, R. Gupta, Y.-X. Jiang, M. Medarde, X. Wu, H. C. Lei, J. Chang, P. Dai, Q. Si, H. Miao, R. Thomale, T. Neupert, Y. Shi, R. Khasanov, M. Z. Hasan, H. Luetkens, and Z. Guguchia, *Nature* **602**, 245 (2022).
- [16] Q. Xiao, Y. Lin, Q. Li, X. Zheng, S. Francoual, C. Plueckthun, W. Xia, Q. Qiu, S. Zhang, Y. Guo, J. Feng, and Y. Peng, *Physical Review Research* **5**, L012032 (2023).
- [17] B. R. Ortiz, P. M. Sarte, E. M. Kenney, M. J. Graf, S. M. L. Teicher, R. Seshadri, and S. D. Wilson, *Physical Review Materials* **5**, 034801 (2021).
- [18] X. Y. Feng, Z. Zhao, J. Luo, J. Yang, A. F. Fang, H. T. Yang, H. J. Gao, R. Zhou, and G.-q. Zheng, *npj Quantum Materials* **8**, 23 (2023).
- [19] J. Frassinetti, P. Bonfà, G. Allodi, E. Garcia, R. Cong, B. R. Ortiz, S. D. Wilson, R. De Renzi, V. F. Mitrović, and S. Sanna, *Physical Review Research* **5**, L012017 (2023).